PCCP

Accepted Manuscript

ROYAL SOCIETY OF CHEMISTRY

www.rsc.org/pccp

Cite this: DOI: 10.1039/c0xx00000x

www.rsc.org/xxxxxx

ARTICLE TYPE

Excitonic energy transfer in polymer wrapped carbon nanotubes in gradually grown nanoassemblies

Victor A. Karachevtsev,[c] Alexander M. Plokhotnichenko [c], Alexander Yu. Glamazda [c,d], Victor S. Leontiev [c] and Igor A. Levitsky *[a,b]

DOI: 10.1039/b000000x

We investigate the exciton energy transfer (ET) in nanoassemblies (nanotube based aggregates) formed by polymer wrapped single walled carbon nanotubes (SWNTs) using photoluminescence (PL) spectroscopy and simulation. The distinctive feature of this study is the gradual growth of such nanostructures in aqueous medium induced by increasing the concentration of porphyrin molecules stitching nanotube-polymer complexes in densely packed assemblies. Experimental dependencies of PL intensity on the porphyrin concentration for different types of semiconducting SWNTs demonstrate step-like behavior controlled by the amount of bound nanotubes and are in good agreement with the simulating model. The simulation algorithm determines the criterion of the aggregate formation depending on the number of porphyrin molecules per tube and the cascade exciton energy transfer between neighbor semiconducting nanotubes of different chiralities. Aggregates of small sizes (up to six-eight individual tubes) contain mostly semiconducting species, while aggregates of a larger size (up to several tens tubes) incorporate metallic SWNTs, inducing strong PL quenching. From the fitting procedure, the ET rate of 0.6×10^{10} s^{-1} has been determined which is consistent with the center to center distance (~ 2.3 nm) between adjacent tubes separated by polymer and porphyrin molecules. The threshold of the dimer formation corresponds to one porphyrin molecule per ~ 20 nm of tube lengths that was supported by molecular dynamics simulation. These findings provide insight into ET mechanism in SWNT nanoassemblies of variable sizes, which can be gradually controlled by the external factor (the concentration of porphyrin molecules).

Introduction

Recent advances in single-walled carbon nanotubes (SWNTs) synthesis, purification and isolation have attracted great attention to the investigation of optical properties of individual nanotubes of various chirality and small bundles of the controlled size.[1, 2] One of the interesting effects related to optical characteristics and exciton dynamics of carbon nanotubes is the exciton energy transfer (ET) between individual SWNTs in the bundles (aggregates)[3–18] and the ET between SWNTs and molecular chromophores[19–21]. As a rule, SWNT aggregation results in the effective ET from semiconducting to metallic tubes or impurities significantly reducing the photoluminescence (PL) quantum yield which makes the ET observation in solid films problematic. However, for suspended SWNT aggregates of small size or for aggregates consisting of individual tubes encapsulated with the surfactant or polymers, there is a good chance to investigate the ET effect with the time-resolved luminescence spectroscopy and transient absorption. An especial role in SWNT isolation plays various polymers (e.g. aromatic polymers[22–24] and DNA[8, 25, 26]), allowing for soft wrapping around single nanotube without defects distinct from surfactant-encapsulated SWNTs. As a result, the quantum yield of such polymer wrapped nanotubes can be higher by one order of magnitude as compared with surfactant isolated tubes.[23,27] Accordingly, attractive conditions for investigating the ET effect between nanotubes of different nature (chirality, diameter, metallic or semiconducting) can be realized in the case of aggregates composed of polymer wrapped SWNTs.

Up to date, reported energy transfer rates between SWNTs in aggregates vary in a broad range from relatively slow of ~ 10^{10} s^{-1} [5, 8] to ultra fast exceeding 10^{14} s^{-1} [12] which can be associated with many factors affecting ET process including: SWNT type (chirality, diameter, semiconducting or metallic), the donor-acceptor spectral overlapping, the intertube distance, aggregate size, the exciton localization and its diffusion length, etc. The majority of reported ET rates (~ 10^{10}–10^{12} s^{-1})[3, 7, 14–16] indicate that classical Förster mechanism significantly overestimates (by three order of magnitude) the experimental data and fails to adequately describe the energy transfer between nanotubes separated by a distance of less than 10 *nm*, as it was demonstrated in the theoretical work by Wong et.al.[28] In this model Förster point dipole approximation has been replaced by extended dipoles approach that allows to reach a satisfactory agreement with the experimental data.

As a rule, the investigation of ET between SWNTs has been performed for SWNT pairs[8,10] or nanotube aggregates without control of their size.[5, 9, 11, 12, 14–16], except the Ref.[17]. Indeed, it is very difficult to gradually change the aggregate size from small bundles consisting of dimers and trimers to relatively large assemblies comprised of several tens species.

We have recently observed the aggregation of poly(rC)-wrapped carbon nanotubes induced by cationic porphyrin meso-tetrakis(4-N-methyl-pyridyl)porphine (TMPyP4).[29] It is noteworthy, that studied nanostructures are not typical SWNT aggregates [3-18] as TMPyP4 molecules are inserted between polymer wrapped nanotubes, however for simplicity sake we name them as nanotube based aggregates or aggregates.

Additions of small amount of TMPyP4 (1 μM) into poly(rC)-SWNTs aqueous suspension initiates the formation of aggregates followed by their further growth up to aggregate visualization at concentrations above 10 μM. Thus, the aggregate size can be controlled by an increasing concentration of TMPyP4 molecules. An unusual feature of such assemblies is their long stability in aqueous suspension without quick precipitation as distinct from conventional aggregates of carbon nanotubes.

Here we report an investigation of the excitonic energy transfer between polymer wrapped semiconducting SWNTs of different chiralities in aggregates of various sizes using luminescent spectroscopy. A distinctive feature of this study is the monitoring of PL quenching for different nanotube types in the broad range of aggregate size from small bundles to large assemblies consisting of several tens of species as a result of the gradual increase of TMPyP4 molecules working as a catalyst for aggregate formation. The proposed model considers the mechanism of the aggregate formation and ET between nanotubes in each aggregate followed by the statistical averaging. The computational results are in good agreement with experimental data and allow to estimate the ET rate and nanotube distribution (semiconducting and metallic) over aggregates of different size for specific concentration of TMPyP4 molecules.

Experimental details

Samples preparation

SWNTs produced by CoMoCat method[30] (SG 65 grade, SouthWest Nano Technologies, Inc.) were used without further purification. Semiconducting tubes with (6, 5) chirality prevailed in the starting material and the total content of semiconducting tubes was more than 95%.

Polycytidylic acid potassium salt poly(rC) (Sigma-Aldrich, USA) was selected for preparation of an aqueous suspension of individual SWNTs. This polymer has the strong base stacked ordering and demonstrates effective adsorption on the carbon nanotube surface.[31] The polymers were dissolved in 0.005 mol × $L^{-1}Na^{+}$ cacodylate buffer (pH 7) (Serva, Germany) with 0.005 mol × L^{-1} NaCl. A stable aqueous suspension of SWNTs was prepared by the sonication of nanotube bundles with poly(rC) for 60 min (1 W, 44 kHz). Then the solution was centrifuged at 70 000 g for 40 minutes. After ultracentrifugation, the supernatant was decanted and dialyzed (dialysis tubing with a molecular weight cutoff of 13-14 kDa) against the buffer solution for 36 h to remove free polynucleotides which were not adsorbed by the SWNTs. Tetra-p-tosylate salt of meso-tetrakis(4-N-methyl-pyridyl)porphine (TMPyP4) (Sigma-Aldrich, USA) (Fig. 1) was used to induce aggregation of poly(rC)-wrapped SWNTs in aqueous suspension. The porphyrin concentration was determined spectrophotometrically in water using the extinction coefficient of ε_{424}= 226000 $M^{-1} \times cm^{-1}$ at the Soret band maximum. In titration experiments, the minimal dose of [TMPyP4] was 50 μM (1 μL) which was added into the nanotube suspension (400 μL). Spectroscopic measurements followed after 15 minutes delay which was required to reach the thermodynamic equilibrium. After each addition, the concentration of porphyrin in suspension was determined, taking into account the increase of the water volume. Porphyrin concentration in the suspension varied from 0.3 × 10^{-6} to 1.1 × 10^{-4} M. A solid sample was prepared by a deposition of the nanotube suspension on a quartz substrate and dried under a stream of warm air.

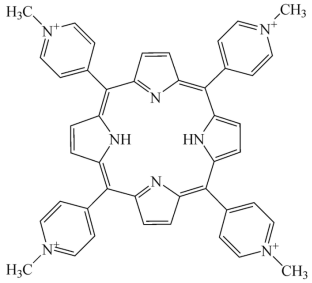

Fig. 1 Molecule structure of TMPyP4

PL measurements and computations

The near-infrared (NIR) PL from semiconducting carbon nanotubes was recorded by a NIR spectrometer with the signal detection by a thermocooled InGaAs photodiode (900−1600 nm). Luminescence was excited with a diode-pumped solid-state green laser (λ_{exc} = 532 nm (2.33 eV), 30 mW).

Computations were carried out on a workstation with processor Pentium-4 using program language Borland C++. For the design of random process of aggregate formation, the generator of pseudorandom numbers from the standard library of functions of Borland C++ v.6.0 was used.

Experimental results

PL from aggregated poly(rC)-SWNTs in aqueous suspension: dependence on TMPyP4 concentration

Fig. 2 shows the dependence of PL spectra of poly(rC)-wrapped SWNTs aqueous suspensions on TMPyP4 concentration which

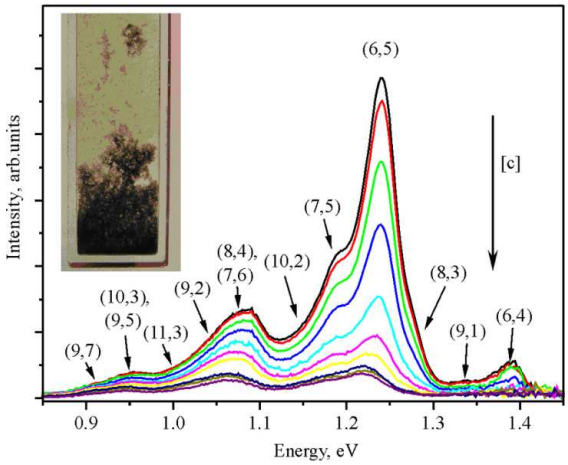

Fig. 2 Emission spectra of semiconducting poly(rC)-wrapped SWNTs in aqueous suspension, obtained using excitation of green laser (λ_{exc} = 532 nm). Arrow indicates the increase of TMPyP4 concentrations, which varied from 0.3 × 10^{-6} to 1.1 × 10^{-4} M. Numbers in brackets denote nanotube chirality. The inset shows the photograph of the water suspension of poly(rC)-SWNT aggregates induced by TMPyP4 at concentration of 1.6 × 10^{-4} M

varied from 0.3 × 10^{-6} to 1.1 × 10^{-4} M. In the PL spectrum, a few bands have been indicative of a few SWNTs with different chiralities and diameters. An increase of TMPyP4 concentration

induces effective PL quenching that accompanies with a red shift for all spectral bands in the range of 0.9−1.4 eV . This suggests that TMPyP4 addition results in gradual aggregate formation, as we observed for absorption spectra earlier. [29] Indeed, at relatively high TMPyP4 concentrations, aggregates are visualized in the form of the floating flakes (Fig. 2, insert). A distinctive feature of poly(rC)-SWNT-TMPyP4 aggregates is a long time stability exhibiting in their floating during several days without quick precipitation.

All PL spectra were fitted with the sum of the minimal number of Lorentzian curves resulting in the band assignment to certain nanotube chirality (it was suggested that FWHM for each band does not exceed 40 meV[32]). The most PL intensive band located at E_{max}= 1.24 eV was assigned to emission from semiconducting tubes with (6,5) chirality which dominates the pristine material. Some of the bands cannot be assigned to SWNTs of definite chirality because their band positions have spectral overlapping with neighbouring bands. Therefore, for two bands, two possible values of chiralities are presented (Fig. 2). Note that TMPyP4 emission does not contribute into the recorded spectra as porphyrin emits in 600−800 nm range (2.08−1.55 eV).[33] Absorbance of TMPyP4 molecules at excitation wavelength (λ=532 nm) is quite weak - less than 3 % of the absorbance of porphyrin solution at the wavelength of the most intensive Soret band (λ=422 nm). Our estimations indicate that the reduction of the energy of excitation light due to TMPyP4 absorption at λ=532 nm is no more than 8% at TMPyP4 concentration of $2*10^{-5}$ M and less than 4% at concentrations of 10^{-5} M and lower. These corrections stay in the limit of the experimental errors which are shown in Fig.3a.

Fig. 3a demonstrates concentration dependences of PL intensity for four bands located at 1.24 eV ((6, 5) chirality), 1.19 eV (7, 5), 1.088 eV ((8, 4) or (7, 9)) and 0.951 eV ((9, 5) or (10, 3)). PL quenching of bands assigned to nanotubes with a larger diameter (lower band gap) is less pronounced as compared with PL quenching for nanotubes with smaller diameters (larger band gap). Additionally, the PL quenching for all type of nanotubes has nonmonotonous character. Such energy dependent PL quenching suggests exciton ET from excited semiconducting nanotube with a larger gap to neighbouring semiconducting nanotube with a smaller gap or to metallic nanotubes. The lowering energy of excited state reduces the number of neighbouring tube-donors and increases the number of tube-acceptors in aggregates leading thus to highest PL quenching for tubes with the largest band gap ((6, 5) tubes in our case). As it was demonstrated in the theoretical study[28] Förster point dipole approximation[34] fails to explain the ET between nanotubes at a distance up to 10 nm and transition monopole approximation (TMA) approach should be applied to correctly predict electronic coupling (see more in discussion section). However, irrelevantly to the ET mechanism, (6, 5) tubes can be considered mostly as energy donor species, (7, 5) tubes as donor and acceptors, and tubes with band at 1.088 eV and 0.951 eV as mostly acceptors. This trend can be clearly seen in Fig. 3 b, where PL concentration dependencies for all types of tubes were normalized on concentration dependency for (6, 5) tubes with highest E_{11} excited energy. Up to 10^{-5} M, ((9, 5) or (10, 3)) tubes with the lowest excited energy exhibits the strongest intensity increase, followed by ((8, 4) or (7, 9)) tubes and (7, 5) tubes. These dependences indicate the cascade ET process from energy donor (6, 5) tubes to other type of tubes in aggregates comprised of donor-acceptor (7, 5) tubes and mostly acceptor tubes ((8, 4) or (7, 9) and (9, 5) or (10, 3)) chiralities. Above 10^{-5} M these dependences change behaviour demonstrating an intensity reduction (Fig. 3 b) that can be associated with domination of PL quenching induced by metallic SWNTs. It is expected that

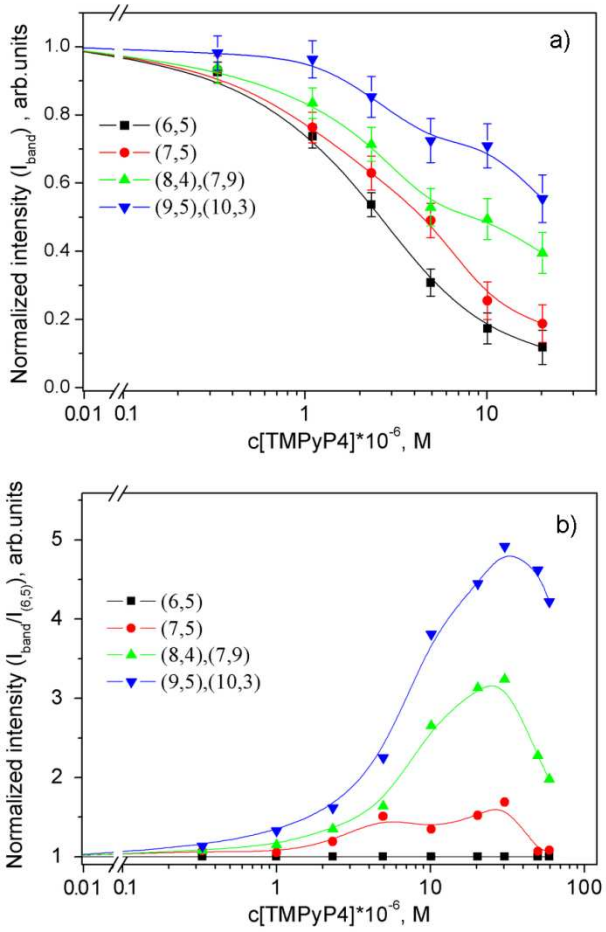

Fig. 3 (a) Concentration dependencies of PL intensity for all nanotube species normalized on initial intensity obtained without TMPyP4; (b) concentration dependencies of PL intensity for all nanotube species normalized on concentration dependence for (6, 5) tubes.

probability to find metallic nanotube in aggregate increases with growth of its size (see also the modelling results and Fig. 7), which is in consistency with Raman spectra for different TMPyP4 concentrations in aqueous suspension and film (see ESI, Fig.1S and text there). Thus, qualitatively we can separate the ET process on two mechanisms at TMPyP4 concentration scale: (**i**) when ET among semiconducting SWNTs prevails over ET between semiconducting and metallic tubes (below TMPyP4 concentration 3×10^{-5} M) and (**ii**) when dominating role plays ET between semiconducting and metallic tubes (above TMPyP4 concentration 3×10^{-5} M). Fig 4 shows the red-shift of the most intensive (6, 5) band in the emission spectrum of poly(rC)-SWNT-TMPyP4 on the porphyrin concentration. Note that the noticeable red-shift is observed at a porphyrin concentration

higher than 10^{-5} M. For example, the band at 1.239 eV is red-shifted up to 35 meV at 10^{-4} M TMPyP4. This dependence indicates the rising interaction among nanotubes in aggregates with the porphyrin concentration. However, the maximal value of this shift is essentially lower than as it was observed under usual nanotube bundle formation which ranged from 70 to 150 meV[35, 36] (depending on nanotube chirality). AFM imaging provides an evidence of individual SWNTs with adsorbed poly(rC) and the beginning of the aggregate formation at low TMPyP4 concentration when polymer-wrapped tubes are assembled in dimers (ESI, Fig. 2S).

PL from SWNT-poly(rC)-TMPyP4 aggregates has also been observed in the solid films formed by the drop cast deposition from aqueous suspension (Fig. 5). It was found that PL spectra of solid film were practically irrelevant to TMPyP4 concentration in nanotube aqueous suspension that can be associated with common thermodynamic conditions (for all TMPyP4 concentrations) affecting aggregate formation during solvent evaporation. This fact indicates that in the solid, there is no opportunity to investigate gradual aggregate growth with an increase of TMPyP4 concentration as in the aqueous medium.

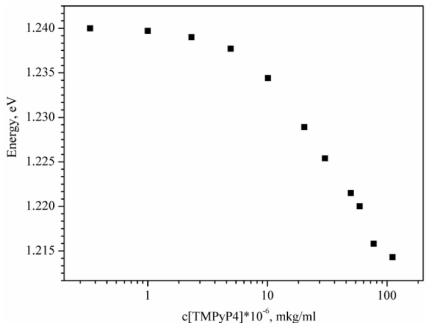

Fig. 4 Dependence of the peak position of the band at 1.239 eV in the emission spectrum of poly(rC)-SWNT-TMPyP4 on the porphyrin concentration.

Similar to absorption spectra,[29] PL bands of different types of aggregated SWNTs in the film are broader by 15−20 meV as compared with nanotube aqueous suspension and can be explained by a stronger interaction between polymer and nanotubes in solid aggregates due to the absence of hydrophobic repulsive forces between the nanotube surface and nitrogen bases of the biopolymer.

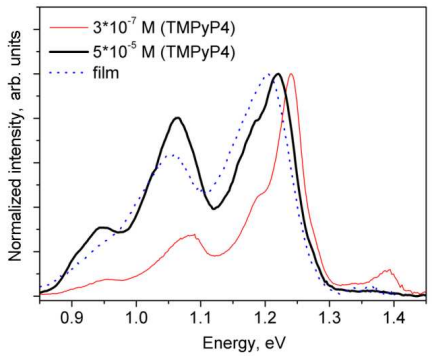

Fig. 5 PL spectra of poly(rC)-SWNT-TMPyP4 aggregates: in the film (blue) and aqueous suspensions for TMPyP4 concentration of 3×10^{-7} M (red) and 5×10^{-5} M (black). All spectra were normalized on the intensity of the most intensive band assigned to (6, 5) nanotubes.

The rough estimates of the efficiency of the ET process in solid film can be done by the comparison of the intensity of low energy PL bands to high energy band (6, 5) tubes (Fig. 5). We can conclude that at first, ET takes place in a solid as this ratio is higher than that for poly(rC)-SWNT in aqueous suspension without TMPyP4 or at low concentration of TMPyP4 (Fig. 5), and second: ET in a solid is less effective than in suspension at high TMPyP4 concentration (the ratio for a solid film is lower as compared with suspension at high TMPyP4 concentration). The later fact is quite interesting and can be interpreted by a lack of the nanotube ordering in solid film and irregular inclusion of metal tubes in contrast to more ordered large aggregates in suspension (closely packed two-dimensional triangular lattice[37]) containing at least one metallic tube (see more details in the next section).

Model

In order to explain the observed PL quenching depending on SWNT chirality, we propose the model taking into account the aggregate formation and ET between individual poly(rC)-wrapped tubes in aggregates followed by statistical averaging.

As distinct from previous studies of ET in SWNT, in our case the TMPyP4 molecules can be considered as catalysts for gradual growth of poly(rC)-SWNT-TMPyP4 aggregates of different sizes from small (dimers, trimers at low TMPyP4 concentration) to large (containing 10−20 tubes at high TMPyP4 concentration). Such unique feature allows filling the gap between extreme limits when only pairs[8, 10] or manifold of tubes in aggregates [5, 9, 11, 12, 14–16] were investigated.

The goal of this simulation is the attempt to reproduce experimental dependencies $R_j(C) = I_j(C)/I_{0j}$ (j =1, 2, 3, 4, see Fig. 3) for four major chiralities/band gaps presented in the PL spectrum (here $I_j(C)$ and I_{0j} is PL intensity with and without TMPyP4, and C is TMPyP4 concentration). The relative quantities of semiconducting SWNTs (Z_j) were determined from deconvoluted PL spectrum (Fig. 2) assuming that the presence of metallic SWNTs (Z_0) is in the range of 0.01−0.05 (1−5 %): [38]

$$Z_j = (1 - Z_0)\frac{S_j}{\sum_{j=1}^{4} S_j} \qquad (1)$$

where S_i is the relative integral intensity of semiconducting SWNTs after spectrum deconvolution. Table I shows values of Z_j, calculated according to Eq.(1) for Z_0 = 0.05 and four different chilarities (E_{11}^{j} is the band gap for first electronic transition).

It was reasonably assumed that the presence of at least one metallic nanotube in aggregate results in complete PL quenching. Thus, aggregates comprised of only semiconducting tubes contribute to PL intensity. The simulation algorithm can be separated by two major parts: (**i**) aggregates formation at determined concentration of TMPyP4 molecules and (**ii**) calculation of PL intensity based on ET process for four nanotube types in each formed aggregate followed by statistical averaging. The details of computational algorithm are presented in ESI.

Table I. Parameters of the model taken from experimental data.

Chirality	j	E_{11}^{j} (eV)	S_j	Z_j
(9, 5), (10, 3)	1	0.951	0.1	0.049
(8, 4), (7, 6)	2	1.088	0.35	0.171
(7, 5)	3	1.19	0.5	0.243
(6, 5)	4	1.24	1.0	0.487

Simulation of aggregates formation

As it was demonstrated in the experiment and molecular dynamics simulation, aggregates of different sizes can be formed with the assistance of TMPyP4 molecules stitching adjacent poly(rC)-SWNT complexes in one nanoassembly (named "unusual aggregate").[29] Molecular dynamics simulation has demonstrated that TMPyP4 molecules work in two ways in the binding process: (**a**) porphyrins couple the polymer-nanotube hybrids through π-π-stacking interaction of the porphyrin core with the nitrogen base or the nanotube surface free from the polymer as well as by the electrostatic interaction between the cationic group of N-methylpyridyl ring and the negatively charged phosphate group of poly(rC), and (**b**) TMPyP4 molecules enhance the polymer coverage of nanotubes as porphyrin adsorbed between neighbor pitches of wrapped polymer reduce the strand sliding [29] . Note that such aggregates can be a result of the fusion of two objects: two individual poly(rC)-SWNT (forming dimer), or one aggregate and one individual poly(rC)-SWNT, either two aggregates of smaller size. An important issue in aggregate assembling is the definition of the fusion criteria (FC) which can be determined by the minimal number of TMPyP4 molecules (C_p) required for the fusion of two objects in one (we neglect the probability of simultaneous fusion of three or more objects in one). Then it is reasonably to assume:

(**i**) C_p is proportional to the number of tubes in the smaller object (it can be individual tube or aggregate) fused with a larger object;

(**ii**) The formation of a new object is controlled by TMPyP4 molecules distributed over surfaces of two fused objects (active molecules which involved in the binding process). The TMPyP4 molecules in the bulk of objects which already engaged in the binding (inactive molecules) are not counted for the fusion criteria (Fig. 6).

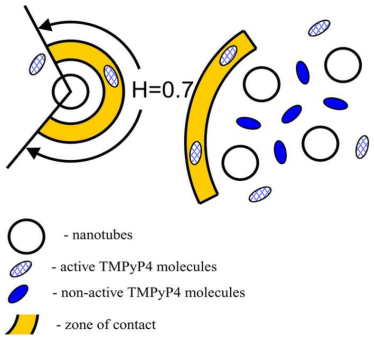

Fig. 6 Schematic view illustrating major parameters for process of aggregate formation.

The surface density (ρ) of active TMPyP4 molecules (C_a) for aggregate containing n_t poly(rC)-SWNT (or n_t tubes) can be determined as:

$$\rho = C_a /(\pi \times L \times d \times n_t^{1/2}),$$

where L is the length and d is the diameter of poly(rC)-SWNT complex. Then the number of active molecules, C_c, in the contact area:

$$S_c = h \times L = \pi \times d \times H \times n_t^{1/2} \times L$$

between larger and smaller objects is the following:

$$C_c = hL(\rho_1 + \rho_2) = (\frac{C_{a1}}{\sqrt{n_{t1}}} + \frac{C_{a2}}{\sqrt{n_{t2}}})H\sqrt{n_{t2}}, \qquad (2)$$

where C_{a1} and C_{a2} are numbers of active molecules and n_{t1} and n_{t2} are numbers of tubes for larger and smaller objects, respectively; H is the parameter of the model defining the width of the contact area S_c (Fig. 6). Finally, in order to satisfy the fusion criteria, the condition $C_c \geq C_p = C_m \times n_{t2}$ should be fulfilled, where C_m is the model parameter (for details, see ESI). Simulation algorithm is designed so that at each fusion event the number of molecules from contact area C_c transit to an inactive status and thus amount of active molecules in the new object C_a is defined as $C_a = C_{a1} + C_{a2} - C_c$.

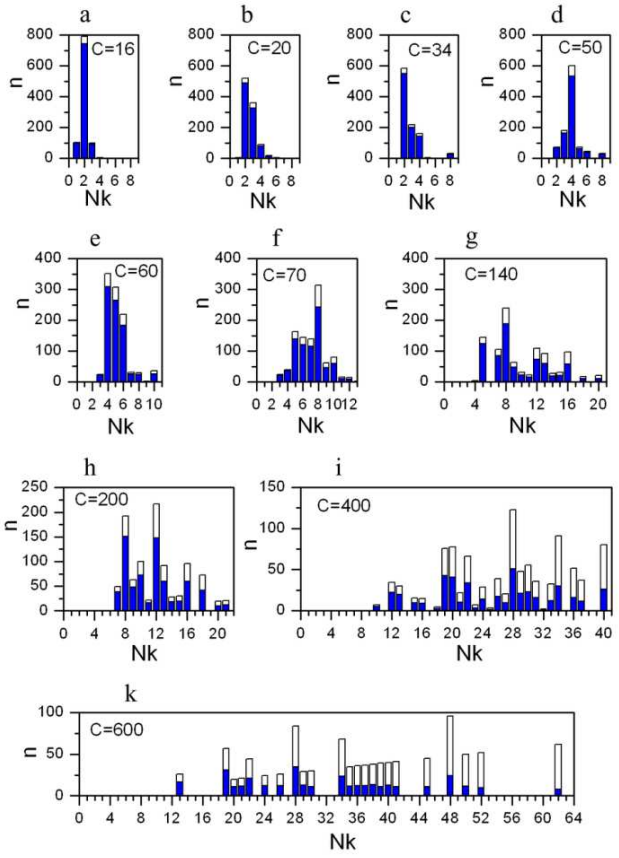

Fig. 7 Diagrams of nanotubes distribution over aggregates (N_K - amount of nanotubes in aggregate) for several concentrations C. Blue and white bars correspond to aggregates with semiconducting nanotubes only and aggregates including metallic tubes, respectively ($Z_0 = 0.03$, $H = 0.7$, $C_m = 20$). Total number of tubes is 1000.

The Fig. 7 demonstrates the simulation of nanotube distribution over aggregates for different values of relative concentration C (average number of TMPyP4 molecules per nanotube). It can be seen, that major contribution in total emission at low and medium concentrations ($C \leq 100$) provides relatively small aggregates (up to 6-8 nanotubes) containing no metallic nanotubes. Because of aggregate compact structure (two dimensional triangular lattice[37]) the distance between any two nanotubes in such aggregates can be considered as constant in the first approximation. Therefore, in further calculation of ET we will omit the dependence of ET on distance between nanotubes.

The PL intensity calculation

After the formation of all aggregates, the next step is calculating the relative PL intensity of each type of semiconducting SWNTs (j=1, 2, 3, 4, see Table I), taking into account the ET rate between them and complete PL quenching for aggregates containing at least one metallic SWNT. As the scaling factor C_m is the model parameter and the average length of nanotubes is not well determined, we employed a relative change of TMPyP4 concentration resulting in PL quenching as a criterion of the model-experiment consistency. The computational formula for $R_j(C)$ (j=1, 2, 3, 4) can be presented as (see ESI):

$$R_j(C) = \frac{1+V_d}{n_j}\sum_j\left(\frac{1+\sum_{i>j}^{4} q_i G_{ij} + \sum_{i>p>j}^{4}\sum_{p>j}^{4} q_i q_p G_{ip} G_{pj} + M}{D_j}\right) \quad (3)$$

, where $M = q_4 \times q_3 \times q_2 \times G_{43} \times G_{32} \times G_{21}$ for j=1 and M=0 for j>1;

$$D_j = 1 + V_d + \sum_{1}^{i<j} q_i V_{ji}\,;\; G_{ij} = V_{ij}/D_j\,;\; n_j = N * Z_j$$

N is the total number of tubes of all types (in the most cases N = 1000), q_i is the number of nanotubes of i-type ($i \neq j$) in each aggregate and Σ_j is the summation of all aggregates without metallic tubes and containing tubes of j type. $V_d = K_d/K_r = (1-\eta)/\eta$ where K^r, K^d, η are radiative and nonradiative rates and the quantum yield of individual poly(rC)-nanotube complex (in the following "nanotube" or "tube"), respectively. $V_{ji} = K_{ji}/K^r$, where K_{ji} is the ET rate from tube j to tube i (i<j), $V_0 = K_{ji}/K^r$ ($i = j$).

We assume for simplicity sake that η, K^d, K^r and V_0 are the same for nanotubes of all types. Because of a sufficiently large center-to-center spacing between adjacent nanotubes separated by wrapped poly(rC) and stitching TMPyP4 molecules (~ 2.3 nm[29]) it was suggested that ET rates (V_0, V_{ji}) are determined by the dipole-dipole coupling. Thus, the short range Dexter mechanism and exciton tunneling[17] can be reasonably excluded. Recently the theoretical work[28] supported by experiments[8, 10, 14–16] demonstrated that the point dipole approximation overestimate significantly the ET rates for distances between tubes up to 10 nm, and the transition monopole approximation (TMA) should be employed for the proper calculation of dipole coupling. In addition, sufficient contribution to overall ET process can be associated not only with donor-acceptor bright excitonic states[28] but also with bright and dark excitonic states. In the later case smaller coupling can be compensated with higher spectral overlapping as it was demonstrated for pair of (7,6) tubes.[28] Thus, the calculation of ET rates in our model based on bright states only (actual overlapping of PL peaks with absorbance peaks for all nanotube types) cannot be quite correct. Therefore, in the first approximation ET rates were set as equal for all nanotube types ($V_0 = V_{ji}$) omitting the overlapping factor. Nevertheless, we tried to compute $R_j(C)$ taking into account spectral overlapping between bright states only and were not able to get a satisfactory agreement with the experimental data (see ESI).

Then the number of variables in the model can be reduced to four parameters: Z_0 is a relative quantity of metallic tubes, H is a parameter defining the contact between two fused objects, η is the quantum yield of single poly(rC)-nanotube complex, and V_0 is the ET rate between any semiconducting SWNTs in the aggregate. Moreover, as simulation for η<<1 shows, ηV_0 value becomes an invariant parameter, which further reduces the number of variables to Z_0, H and V_0 at the fixed η=0.01. Taking into account some relatively rough simplifications in the proposed model, we realized that the exact coincidence of the simulation data with an experiment is hardly can be expected. Therefore, several fitting criteria were introduced. Simulated $R_j(C)$ curves should be satisfied by the following conditions: (1) $R_j(C)$<1 at all j; (2) R_1>R_2>R_3>R_4 at all C; (3) $C(R_4$=0.1)/$C(R_4$=0.9) ≈ 70 and (4) $C(R_4$=0.1)≈$C(R_i$=0.5). For a given set of parameters, the computational cycle was stopped if one of the above conditions was violated and simulation procedure started over for the next set of parameters.

Discussion

The $R_i(C)$ functions calculated for several Z_0 values in the range of 0.01>Z_0>0.06, η=0.01 (the quantum yield of 1% for individual tube was reported in Ref. 5), H=0.7 and optimal V_0 values are shown in Fig. 8 (the optimal V_0 was chosen at minimal mean deviation from the experimental data point at each Z_0 fixed). It is noteworthy that simulated PL quenching for all types of semiconducting nanotubes displays non-monotonous reduction and shows several steps at increasing TMPyP4 concentration. An initial slope (up to C=20) can be interpreted by the dimer formation (Fig. 7a) followed by the plateau (20<C<40) which is consistent with Fig. 7b,c indicating that at these concentrations the aggregates size is almost unchanged (the range of dimer and trimer domination).

At C ~50−80, the $R_i(C)$ slope increases sharply that can be associated not only with the rapid growth of aggregates of larger sizes (where 5-mers and 6-mers dominate) but also with higher contribution of aggregates containing metallic nanotubes (Fig. 7d,e,f). This fact suggests that the non-monotonous aggregate growth (with enriched metal nanotubes at higher C) results in step-like features in $R_j(C)$ dependencies. It is remarkable that the similar non-monotonous quenching is also observed in the experiment for all four types of semiconducting tubes (Fig. 3, and the same data points shown in Fig. 8), that is in an agreement with our model. The singularity (the slope change) on experimental $R_j(C)$ curves appears at TMPyP4 concentration of ~ $(3-4) \times 10^{-6}$ M. Then taking the nanotube concentration of 2.5 ×

10^{-3} M of carbon atoms (2.5×10^{21} carbon atoms/L), an average number of 700 carbon atoms per one TMPyP4 molecule can be estimated as a rough criterion of the dimer and trimer formation. For example, for (6, 5) nanotubes it corresponds to one TMPyP4 molecule per ~20 nm of the tube's length. This value is consistent with MD simulation predicting one TMPyP4 molecules per 17 nm of SWNT (10, 0) wrapped by poly(rC) is sufficient to form a stable dimer.[29]

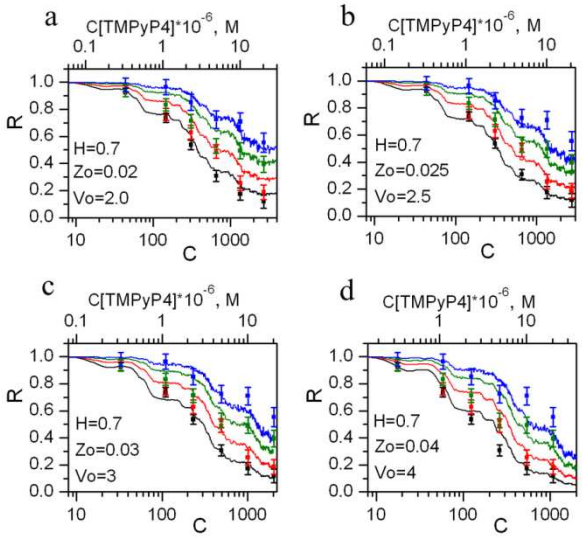

Fig. 8 Calculated $R_i(C)$ functions (lines) for H = 0.7, variable Z_0 and optimal V_0 values and their comparisons with experimental data (dots with error bars). Lower and upper scales correspond with number of TMPyP4 molecules per tube and TMPyP4 suspension concentration in suspension, respectively. The legend of colors is the same as in Fig. 3.

An efficient ET rate can be estimated from the best fitting procedure indicative of parameters Z_0=0.03, V_0=3, η=0.01 (Fig. 8c). For η=0.01, $K_r + K_d = 2 \times 10^{11}$ s^{-1} [39] and V_0=3, we find K_{it}=K_0=0.6×10^{10} s^{-1}, which is one order less of magnitude than ET rate of $0.3 - 5 \times 10^{11}$ s^{-1} between DNA-wrapped (9, 1) and (6, 5) SWNTs[8] with the center to center distance of ~ 1.66 nm. In addition, it was reported that the relatively slow energy transfer between small bundles of SDS wrapped (9, 4) SWNTs as 1.3×10^{10} s^{-1} was estimated from luminescence decay[5]. According to MD simulation, the center to center distance between two poly(rC)-wrapped (10, 0) SWNTs and stitched by four TMPyP4 molecules is ~ 2.3 nm[29]. Then lower transfer rate in our case can be explained by the increase of the center to center distance between adjacent tubes in aggregates. Intuitively, it is expected that introducing TMPyP4 molecules between poly(rC)-wrapped SWNTs should result in the largest center to center distance with respect to DNA-wrapped SWNT[8] and SWNT bundles.[5, 9, 12, 16, 18]

Also, the presence of TMPyP4 molecules between poly(rC)-SWNTs in the aggregate should not only increase the inter-tube distance, but also modify the nature of the energy transfer process due to the gradient of the electric field and high polarizability in the vicinity of ionic TMPyP4 molecules. Indeed, taking our estimate of 20 nm of the tube length per one TMPyP4 molecule at the beginning of the dimer/trimer formation and the exciton diffusion length of 100-200 nm,[40–42] we can suggest that photogenerated exciton encounters several times with strong polarization singularity localized at TMPyP4 molecule. As a result, Coulomb coupling can be significantly changed, affecting the ET rate. Note, that such a scenario suggests the dependence of the ET rate on TMPyP4 concentration, as the number of exciton encounters increases with the amount of TMPyP4 molecules distributed over the nanotube. Probably, the TMA model[28] that is often employed for the interpretation of recent experimental results of ET in SWNT aggregates cannot be directly applied to this case and further modification is required.

Conclusion

In summary, we have investigated the exciton energy transfer in polymer-wrapped SWNT based aggregates by PL spectroscopy and modeling. A distinctive property of such nanoassemblies is the presence of cationic porphyrin molecules stitching individual SWNTs with wrapping anionic poly(rC) in quasi-ordered aggregates. Such a unique feature allows controlling gradually the aggregate growth from small species (dimers, trimers) to relatively large ones (comprised of several tens of tubes) by simple variation of TMPyP4 concentration in aqueous medium. Thus, the ET process can be carefully monitored over the whole scale of aggregate magnitude. It is noteworthy that the most of previous studies of ET in carbon nanotubes[5–16,18] dealt with pairs of tubes or with bundles/aggregates of the uncontrolled size. The proposed model is comprised of two main procedures: (**i**) the aggregate formation and (**ii**) the ET between individual poly(rC)-wrapped tubes in aggregates followed by statistical averaging. In particular, the aggregate growth has been determined as a function of TMPyP4 molecules distributed over the contact area (active molecules) between two fused objects (smaller aggregates or individual poly(rC)-SWNT complexes) while TMPyP4 molecules in the bulk of the objects were not counted for fusion criterion (inactive molecules). Despite several simplifications (e.g. omitting the ET dependence on distance, spectral overlapping for pairs of donor-acceptor tubes) we have reached a remarkable similarity of modeling with experimental data. Moreover, the model was able to reproduce step-like behavior of PL intensity on TMPyP4 concentration for all types of semiconducting carbon nanotubes, which presumably is associated with the discrete character in the aggregate formation. The relatively low ET rate of 0.6×10^{10} s^{-1} can be explained by the large center to center distance between adjacent polymer wrapped nanotubes (~ 2.3 nm) and insertion of TMPyP4 molecules. Also, it was found that one TMPyP4 molecules per ~ 20 nm of the nanotube length is sufficient for the initiation of stable poly(rC)-SWNT dimer, which is in excellent agreement with our previous molecular dynamics simulations.[29] Beyond the unique structure of SWNT-polymer-molecule hybrids, this work demonstrates the fundamental understanding of ET process in small clusters produced by controlled aggregation of polymer wrapped carbon nanotubes which can be employed in the future research of various multifunctional nanoassemblies in optoelectronics, photovoltaics and nanobiotechnology.

Notes and references

[a] *Emitech, Inc. Fall River, MA 02720, USA. E-mail: ilevitsky@emitechinc.com*

[b] Department of Chemistry, University of Rhode Island, Kingston, RI 02881, USA. E-mail: ilevitsky@chm.uri.edu
[c] B.I. Verkin Institute for Low Temperature Physics and Engineering, National Academy of Sciences of Ukraine, Kharkov, 61103, Ukraine.
[d] Department of Physics, Chung-Ang University, 221 Huksuk-Dong, Seoul 156-756, Republic of Korea

† Electronic Supplementary Information (ESI) available: [details of any supplementary information available should be included here]. See DOI: 10.1039/b000000x/

References

1 M. J. O'Connell, S. M. Bachilo, C. B. Huffman, V. Moore, M. S. Strano, E. Haroz, K. Rialon, P. J. Boul, W. H. Noon, C. Kittrell, J. Ma, R. H. Hauge, R. B. Weisman and R. E. Smalley, *Science,* 2002, **297**, 593-596.
2 *Carbon Nanotubes: Advanced Topics in Synthesis, Properties, and Applications*, ed. A. Jorio, M. S. Dresselhaus, and G. Dresselhaus, Springer, Berlin, 2008.
3 A. Maeda, S. Matsumoto, H. Kishida, T. Takenobu, Y. Iwasa, H. Shimoda, O. Zhouand, M. Shiraishi and H. Okamoto, *J. Phys. Soc. Jpn.,* 2006, **75**, 043709.
4 O. N. Torrens, D. E. Milkie, M. Zheng and J. M. Kikkawa, *Nano Lett.,* 2006, **26**, 2864-2867.
5 S. Berger, C. Voisin, G. Cassabois, C. Delalande, P. Roussignol and X. Marie, *Nano Lett.*, 2007, **7**, 398-402.
6 J. Crochet, M. Clemens and T. Hertel, *J. Am. Chem. Soc.*, 2007, **129**, 8058-8059.
7 P. H. Tan, A. G. Rozhin, T. Hasan, P. Hu, V. Scardaci, W. I. Milne and A. C. Ferrari, *Phys. Rev. Lett.,* 2007, **99**, 137402.
8 H. Qian, C. Georgi, N. Anderson, A. A. Green, M. C. Hersam, L. Novotny and A. Hartschuh, *Nano Lett.,* 2008, **8**, 1363-1367.
9 T. Kato and R. Hatakeyama, *J. Am. Chem. Soc.,* 2008, **130**, 8101-8107.
10 J. Lefebvre and P. Finnie, *J. Phys. Chem. C,* 2009, **113**, 7536-7540.
11 F. Chen, J. Ye, M. Y. Teo, Y. Zhao, L. P. Tan, Y. Chen, M. B. Chan-Park and L.-J. Li, *J. Phys. Chem. C*, 2009, **113**, 20061-20065.
12 L. Lüer, J. Crochet, T. Hertel, G. Cerullo and G. Lanzani, *ACS Nano,* 2010, **4**, 4265-4273.
13 H. Hirori, K. Matsuda and Y. Kanemitsu, *Phys. Rev. B*, 2008, **78**, 113409.
14 T. Koyama, K. Asaka, N. Hikosaka, H. Kishida, Y. Saito and A. Nakamura, *J. Phys. Chem. Lett.,* 2011, **2**, 127-132.
15 T. Koyama, Y. Miyata, Y. Asada, H. Shinohara, H. Kataura and A. Nakamura, *J. Phys. Chem. Lett.,* 2010, **1**, 3243-3248.
16 T. Koyama, Y. Asada, N. Hikosaka, Y. Miyata, H. Shinohara and A. Nakamura, *ACS Nano*, 2011, **5**, 5881-5887.
17 J. J. Crochet, J. D. Sau, J. G. Duque, S. K. Doorn and M. L. Cohen, *ACS Nano,* 2011, **5**, 2611-2618.
18 R. D. Mehlenbacher, M.-Y. Wu, M. Grechko, J. E. Laaser, M. S. Arnold and M. T. Zanni, *Nano Lett.,* 2013, **13**, 1495-1501.
19 A. Ahmad, T. Kurkina, K. Kern and K. Balasubramanian, *ChemPhysChem,* 2009, **10**, 2251-2255.
20 C. Roquelet, B. Langlois, F. Vialla, D. Garrot, J. Lauret and C. Voisin, *Chem. Phys.,* 2013, **413**, 45-54.
21 T. Heek, A. Setaro, R. Haag and S. Reich, *Adv. Funct. Mater.,* 2012, **22**, 3921-3926.
22 F. Chen, B. Wang, Y. Chen and L.-J. Li, *Nano Lett.,* 2007, **7**, 3013-3017.
23 A. Nish, J.-Y.Hwang, J. Doig and R. J. Nicholas, *Nat. Nanotechnol.,* 2007, **2**, 640-646.
24 J.-Y. Hwang, A. Nish, J. Doig, S. Douven, C.-W. Chen, L.-C. Chen and R. J. Nicholas, *J. Am. Chem. Soc.,* 2008, **130**, 3543-3553.
25 M. Zheng, A. Jagota, M. S. Strano, A. P. Santos, P. Barone, S. G. Chou, B. A. Diner, M. S. Dresselhaus, R. S. Mclean, G. B. Onoa, G. G. Samsonidze, E. D. Semke, M. Usrey and D. J. Walls, *Science,* 2003, **302**, 1545-1548.
26 I.A Levitsky, W.B. Euler, and V.A. Karachevtsev, *Photophysics of carbon nanotubes interfaced with organic and inorganic Materials*, Springer-Verlag, London, 2012.
27 J. Lee, X. Wang, L. J. Carlson, J. A. Smyder, B. Loesch, X. Tu, M. Zheng and T. D. Krauss, *Nano Lett.,* 2011, **11**, 1636-1640.
28 Y. Wong, C. Curutchet, S. Tretiak and G. D. Scholes, *J. Chem. Phys.,* 2009, **130**, 081104.
29 E. S. Zarudnev, A. M. Plokhotnichenko, V. S. Leontiev, I. A. Levitsky and V. A. Karachevtsev, *J. Mater. Chem.,* 2012, **22**, 10795-10804.
30 W. E. Alvarez, F. Pompeo, J. E. Herrera, L. Balzano and D. E. Resasco, *Chem. Mater.,* 2002, **14**, 1853-1858.
31 M. V. Karachevtsev, G. O. Gladchenko, A. M. Plokhotnichenko, V. S. Leontiev and V. A. Karachevtsev, *J. Phys. Chem. B,* 2013, **117**, 2636-2644.
32 C. Fantini, V. Jorio, A. P. Santos, V. S. T. Peressinotto and M. A. Pimenta, *Chem. Phys. Lett.,* 2007, **439**, 138-142.
33 R. F. Pasternack, C. Bustamante, P. J. Collngs, A. Giannetto and E. J. Gibbs, *J. Am. Chem. Soc.,* 1993, **115**, 5393-5399.
34 T. Förster, *Discuss. Faraday Soc.,* 1959, **27**, 7-17.
35 J. S. Park, Y. Oyama, R. Saito, W. Izumida, J. Jiang, K. Sato, C. Fantini, A. Jorio, G. Dresselhaus and M. S. Dresselhaus, *Phys. Rev. B,* 2006, **74**, 165414.
36 S. K. Doorn, *J. Nanosci. Nanotech.,* 2005, **5**, 1023-1034.
37 A. Thess, R. Lee, P. Nikolaev, H. Dai, P. Petit, J. Robert, C. Xu, Y. H. Lee, S. G. Kim, A. G. Rinzler, D. T. Colbert, G. E. Scuseria, D. Tomanek, J. E. Fischer and R. E. Smalley, *Science,* 1996, **273**, 483-487.
38 "Southwest nanotechnologies, inc.", http://swentnano.com/tech/docs/TD_SG65i.pdf.
39 F. Schöppler, N. Rühl and T. Hertel, *Chem. Phys.,* 2013, **413**, 112-115.
40 J. Siitonen, D. A. Tsyboulski, S. M. Bachilo and R. B. Weisman, *J. Phys. Chem. Lett.,* 2010, **1**, 2189-2192.
41 C. Georgi, M. Bohmler, H. H. Qian, L. Novotny and A. Hartschuh, *Solid State Phys.,* 2009, **246**, 2683-2688.
42 K. Yoshikawa, K. Matsuda and Y. Kanemitsu, *J. Phys. Chem. C,* 2010, **114**, 4353-4356.